Production of Extended Single-Layer Graphene

Mingsheng Xu,[†,‡,*] Daisuke Fujita,[§,⊥] Keisuke Sagisaka,[§] Eiichiro Watanabe,[∥] and Nobutaka Hanagata[∥,#]

[†]International Center for Young Scientists, National Institute for Materials Science, 1-2-1 Sengen, Tsukuba, Ibaraki 305-0047, Japan, [‡]MOE Key Laboratory of Macromolecule Synthesis and Functionalization, State Key Laboratory of Silicon Materials, and Department of Polymer Science and Engineering, Zhejiang University, Hangzhou 310027, P. R. China, [§]Advanced Nano Characterization Center, [⊥]International Center for Materials Nanoarchitectonics, and [∥]Nanotechnology Innovation Center, National Institute for Materials Science, 1-2-1 Sengen, Tsukuba, Ibaraki 305-0047, Japan, and [#]Graduate School of Life Science, Hokkaido University, Sapporo, Japan

ABSTRACT Graphene has attracted an enormous amount of interest recently because of its unique electronic, optical, mechanical, and other properties. We report a promising method for producing single-layer graphene fully covering an entire substrate at low temperature. Single-layer graphene sheets have been synthesized on a whole 2 cm × 2 cm nickel (Ni) film deposited on a highly oriented pyrolytic graphite (HOPG) substrate by heating the Ni/HOPG in a vacuum. The carbon atoms forming our graphene are diffused from the graphite substrate through the nickel template. Our results demonstrate how to control the amount of carbon atoms for graphene formation to yield graphene films with a fine controlled thickness and crystal structure. Our method represents a significant step toward the scalable synthesis of high-quality graphene films with predefined thickness and toward realizing the unique properties of graphene films.

KEYWORDS: graphene · nickel · epitaxial growth · monolayer graphene · highly oriented pyrolytic graphite

Graphene has recently attracted a great deal of interest in both academia and industry because of its unique electronic[1] and optical properties.[2] The superb characteristics of graphene make this material one of the most promising candidates for various applications, such as ultrafast electronic circuits[1,3] and photodetectors,[2] clean and renewable energy,[4] and rapid single-molecule DNA sequencing.[5] The electronic properties of graphene systems heavily rely on the number of graphene layers,[6] on their intrinsic defects,[7] and on the coupling of the graphene sheet with the underlying substrate.[1] Fine control over the thickness and the crystalline structure of graphene layers is essential to realize the unique properties of graphene. Graphene films can be produced by mechanical exfoliation of graphite,[1] solution approaches,[8,9] thermal decomposition of silicon carbide (SiC),[10,11] chemical vapor deposition (CVD),[12−15] and segregation on catalytic metals.[16−18] Among these methods, CVD and carbon segregation from a solid source are promising approaches to generate large scale graphene layers with high quality. For instance, monolayer graphene with coverage of more than 95% on Cu foils[15,19,20] have been reported. Millimeter-scale monolayer graphene was synthesized on a Ru(0001) single crystal.[21,22] Bilayer and multilayer graphene can be synthesized on single crystalline SiC.[10,11] Despite these significant advances in the synthesis of large-area graphene, few-layer graphene or graphene islands on monolayer graphene have been often observed instead of monolayer graphene with high uniformity. Particularly, the maximum coverage of monolayer graphene on a nickel (Ni) substrate[19] is less than 20%. The variability in the thickness of graphene layers and graphene grains over the same substrate leads to fluctuations of the electric transport properties of graphene,[3,14,15] thus preventing us from taking advantage of the distinct properties of monolayer graphene for practical large-scale integrated applications.

Among the substrates used for the synthesis of graphene,[12−26] the Ni(111) surface provides one of the best templates, due to small lattice mismatches of this surface with the graphene structure.[16,17] This property makes Ni(111) one of the most promising catalytic metals for commensurate epitaxial growth of structurally homogeneous graphene, and it accounts for the excellent physical properties shown by graphene grown on Ni(111), most notably the quantum Hall effect.[14] However, there is an intrinsic difficulty in synthesizing monolayer graphene on Ni(111) due to a large solubility of carbon inside the Ni substrate. Here, we report on centimeter-scale synthesis of single-layer graphene on a nickel surface deposited on a highly oriented pyrolytic graphite (HOPG) substrate by the diffusion of carbon atoms through the nickel

*Address correspondence to msxu@zju.edu.cn, XU.Mingsheng@nims.go.jp.

Received for review December 13, 2010 and accepted January 6, 2011.

Published online January 12, 2011
10.1021/nn103428k

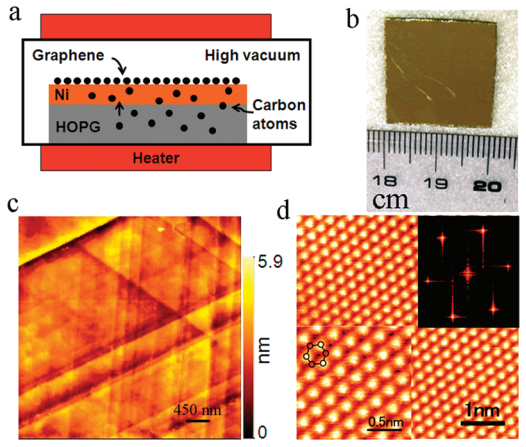

Figure 1. Novel Ni(111)/HOPG(0001) system for production of high-quality single-atomic graphene layer: (a) schematic diagram of graphene growth system and formation mechanism; (b) graphene on Ni(111)/HOPG(0001) (size: 2 cm × 2 cm); (c) AFM image of our graphene sheet; (d) constant current STM image of our graphene sheet. The top-right and bottom-left insets show a two-dimensional fast Fourier transform taken from the STM image and STM image superimposed by the honeycomb lattice of graphene, respectively.

template. Our results demonstrate how optimization of the relevant parameters for producing the graphene—annealing time and temperature—yields a fine control of thickness and structure of the graphene layer. Our method represents a significant step toward the scalable synthesis of graphene films with high structural quality and finely controlled thicknesses and toward realizing the unique properties of graphene.

RESULTS AND DISCUSSION

To solve the problem of large solubility of carbon inside a Ni substrate and to realize commensurate epitaxial growth of metal templates and of subsequent graphene, we epitaxially grow a Ni(111) surface on an HOPG(0001) surface (see Supporting Information, Figure S1) and produce a single-atomic layer graphene on top of this Ni template by controlling the diffusion of carbon atoms from the HOPG(0001) through the Ni layer (Figure 1a) in high vacuum conditions (see Methods). Figure 1b shows one of the typical graphene samples that we prepared with this method. It has a size of 2 cm × 2 cm, and the protruding flakes are due to a mechanical cleavage of the HOPG substrate. An atomic force microscopy image of one of these single-layer graphene samples grown on a Ni(111)/HOPG-(0001) template over a 4.5 μm × 4.5 μm scan area is displayed in Figure 1c. This image shows a vertical corrugation of ~5.9 nm and a root-mean-square roughness of ~6.9 Å over the whole image due to the interface among the percolated Ni(111) islands composing the Ni(111) template. The root-mean-square roughness of the flat areas on top of the Ni(111) grains has a typical value of ~3.2 Å, that points to a smooth graphene layer grown on top of the Ni substrate. A typical scanning tunneling microscopy image (local density of states) of our samples (Figure 1d) shows one of the two sublattices of the honeycomb structure of the sample on the Ni/HOPG, with a measured lattice constant of 2.4 ± 0.2 Å; although the distance between the carbon atoms in graphene is ~1.4 Å, in our STM images one of the sublattices is missing, in good agreement with previous observations.[27,28] These measurements suggest that our sample is graphene and a high-quality graphene layer grown on the Ni(111)/HOPG(0001) template.

Raman spectroscopy has shown to be a powerful tool to count graphene layers,[29] and we have used this technique to characterize our graphene samples. However, due to a relatively strong electronic coupling between the graphene and the Ni substrate,[30] we did not detect any Raman characteristics between 1000 and 3500 cm^{-1} when using 532 and 514 nm excitation lasers. As an alternative tool, we used scanning Auger electron spectroscopy (AES)[10,17,18] simultaneously with scanning electron microscopy (SEM) to evaluate the uniformity and thickness of the our graphene samples (Figure 2). Here, we have measured the KLL Auger electron transition of carbon (C KLL) and the LMM and MVV Auger transitions of nickel (Ni LMM and Ni MVV, respectively). The identical intensity of the C KLL signal (Figure 2g) suggests a uniform thickness of our graphene samples covering the whole Ni substrate. A typical SEM image of our samples (Figure 2a) revealed the presence of Ni grains with different color contrasts and steps, as well as dark hole-like defects and small very bright protrusions (see Supporting Information, Figures S2−S3). The small dark spot pointed by an arrow in the SEM image (Figure 2a) displays the brightest feature in the map for the C KLL transition (Figure 2c) over the sampled area. Although the C KLL map does display a slight color contrast in the brighter and darker regions, the peak-to-peak magnitudes of C KLL (Figure 2g) and Ni MVV transition spectra (Figure 2f) taken over different regions of the sample show a negligible variation, in contrast to considerable changes of the Ni LMM transition spectra (Figure 2h). According to this intensity variation, the Ni LMM map (Figure 2d) shows strong contrast between the brighter and darker regions in the SEM image (Figure 2a), where the spectra were taken (see the areas highlighted with circles), indicating that the contrast difference in the SEM image mainly stemmed from different electron emissions from the underlying Ni grains showing different crystalline orientations (see Supporting Information and relevant discussion, Figure S4) at an ~10 kV acceleration voltage. The different Ni LMM transition intensities may be due to channeling effects stemming from different orientations deviating from the Ni(111) direction. For instance, in the case of the Ni/HOPG substrate annealed for ~23 h at 650 °C, the crystal orientation of all grains is seemingly in the Ni(111) direction (see Supporting Information, Figure S4b,c). However, with respect to the Ni(111) direction (see

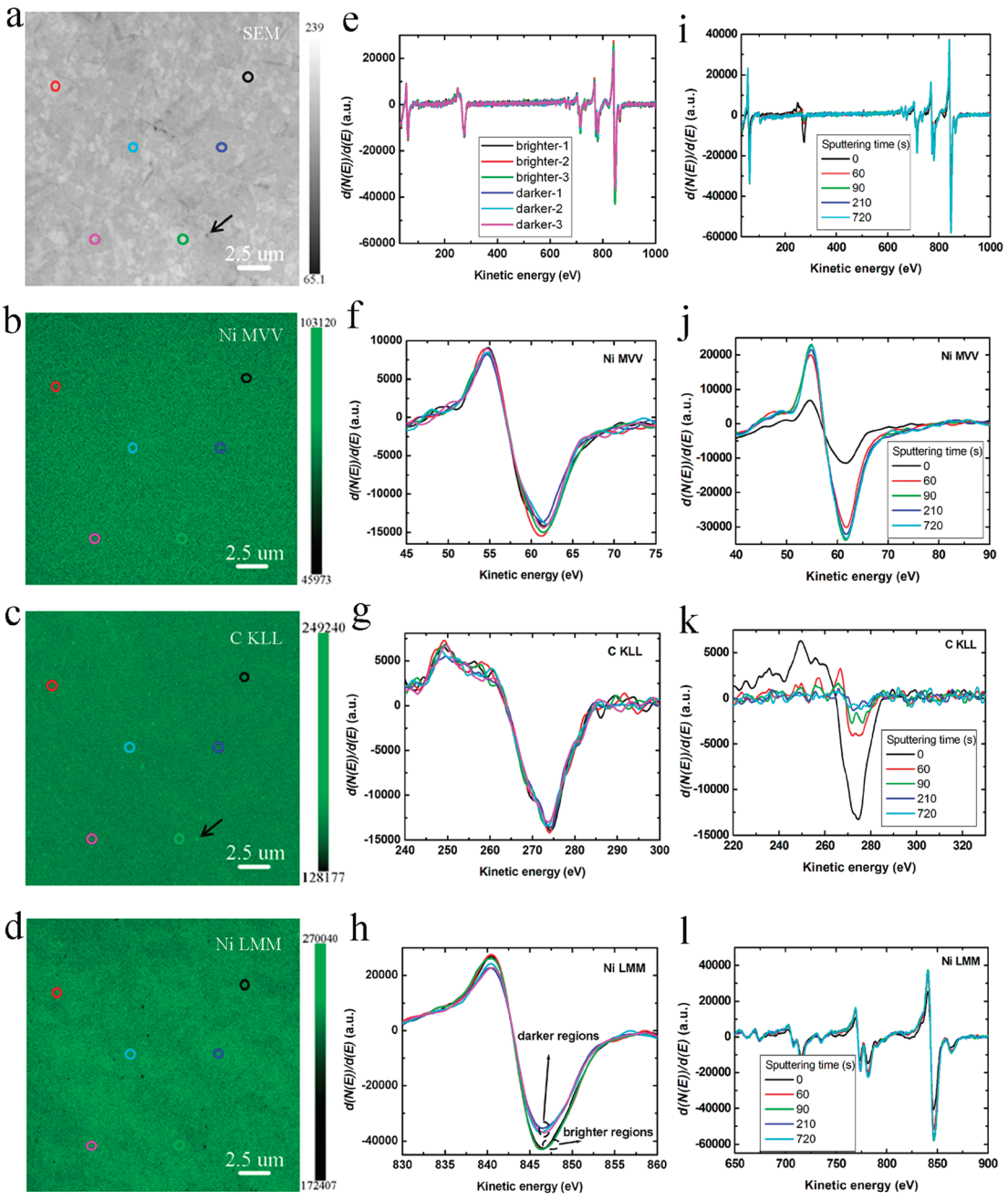

Figure 2. AES characterization of a graphene sheet grown on Ni(111)/HOPG(0001): (a) SEM image, showing brighter and darker grains, as well as small dark spots indicated by the arrow; (b) Ni MVV Auger electron map; (c) C KLL Auger electron map; (d) Ni LMM Auger electron map. (e−h) AES differential spectra of a graphene sheet obtained from various brighter and darker regions marked with corresponding colored circles in panels a−d: (e) survey spectra; (f) Ni MVV spectra; (g) C KLL spectra, showing no intensity change in the brighter and darker regions; (h) Ni LMM spectra, showing variation of intensity in the brighter and darker regions. (i−l) Evolution of Auger electron intensity of graphene layer with sputtering time: (i) survey spectra; (j) Ni MVV spectra; (k) C KLL spectra; (l) Ni LMM spectra. After ~90 s of sputtering the sample, a C KLL signal was still detected.

Supporting Information, Figure S4e−g), 72.5% of grains were oriented in a range from 0° to 1°, 26.7% of grains were in a range from 1° to 2°, and 0.7% were in a range from 2° to 3°. The results suggest that our graphene sample has a uniform thickness except for a few localized brightest spots, of which one is pointed to by an arrow (Figure 2c), regardless of the brighter and darker Ni grains observed in the SEM image. However, if the Ni grain boundaries are present, this may lead to inhomogeneity of the graphene synthesis (see Supporting Information, Figure S5).

To understand the growth dynamics and to determine the thickness of our graphene sheet grown on a Ni(111)/HOPG(0001) template, the sample was worn down by ion-gun sputtering, and AES spectra were acquired at several time intervals during the abrading process (Figure 2i−l). After 60 s sputtering, the peak intensity of the C KLL transition decreased to 43% of its

original magnitude (Figure 2k), while the peak intensities of Ni MVV (Figure 2j) and Ni LMM (Figure 2l) transitions increased 274% and 129%, respectively, with respect to their initial values. Further changes along the same trend were observed with an additional 30 s of sputtering time. After a total of ~90 s sputtering of the sample, the intensities of these transitions barely changed, and a carbon signal was still detected (Figure 2k). We believe that this signal corresponds to carbon atoms embedded in the Ni substrate (see Supporting Information, Figure S6). These observations indicate that the formation of our graphene sheet on Ni(111)/HOPG(0001) is different from the growth mechanism of graphene on copper,[15] and from the synthesis of graphene films on Ni based on other methods such as CVD[13,14] and segregation.[12,16,17] The carbon atoms that form our graphene layer are controlled by the HOPG substrate by a diffusion process through the Ni template, which is the difference, that is, how to control carbon to dissolve in the bulk of Ni film and how much carbon atoms dissolved in the Ni template. Segregation of these carbon atoms from the Ni film, nucleation at the Ni grain boundaries, and finally diffusion of carbon atoms on the Ni(111) surface further controls the formation of our graphene layer. These dynamic processes depend very much on the time and annealing temperature of the sample during the preparation process; parameters that together with the saturation solubility[15] of carbon in Ni—significantly less than 0.1% in weight after annealing a Ni thin film at 650 °C (ref 31) (see Supporting Information, Figure S6)—are critical for the formation of the our graphene samples.

We used a standard attenuation model[32,33] to estimate the thickness of our graphene sheet grown on Ni(111)/HOPG(0001). Because low-energy electrons are more sensitive to surface changes, the peak-to-peak magnitude of the Ni MVV transition (Figure 2j) was used for calculating the thickness of the graphene layer according to this elemental relation:[33]

$$I_{sub} = I_{sub,\,pure} \exp[-(nd_0)/\lambda \sin(\theta)] \qquad (1)$$

where I_{sub} is the peak-to-peak magnitude of the Ni MVV transition prior to wearing down the sample by ion-gun sputtering, $I_{sub,pure}$ is the peak-to-peak magnitude of the Ni MVV peak after removing the graphene layer (*i.e.*, 700 s sputtering time), n is the number of graphene layers, d_0 is the theoretical thickness of graphene (3.35 Å), θ is the electron takeoff angle (42° for the present Auger instrument), and λ is the inelastic mean free path (IMFP) of the Auger electrons for graphene. We have used a value of 4.5 Å as the IMFP for the electron energy of the Ni MVV transition that we recently derived for graphene.[32] By applying this IMFP value and the intensities of Ni MVV transition peaks to the equation, the thickness of the our graphene layer grown on Ni(111)/HOPG(0001) was calculated to be 3.1 Å, suggesting a single-atomic graphene layer. This thickness value is smaller than the interlayer spacing between two graphene layers in graphite (3.35 Å), yet reasonable considering the orbital hybridization at the interface between graphene and Ni.[30]

To further identify our sample as graphene and confirm that our graphene sheet grown on Ni(111)/HOPG(0001) is a single-atomic layer of graphene, we transferred the graphene sheet from the Ni substrate on a silicon substrate coated with a SiO_2 layer, and then characterized it with Raman spectroscopy (Figure 3). The Raman spectra show typical features of monolayer graphene:[29] a symmetric 2D band centered at ~2680 cm^{-1} with a full width at half-maximum (fwhm) of ~40 cm^{-1}, a G band centered at ~1580 cm^{-1}, and a G/2D intensity ratio of ~0.31. A total of 100 Raman spectra were randomly collected from a Raman map acquired over a 90 μm × 90 μm area of the sample, and all of them showed such single-layered graphene characteristics. Several Raman maps were collected over different locations of the sample, producing identical results and an average G/2D intensity ratio of ~0.31 ± 0.03 (Figure 3d). All this experimental evidence indicated that we had synthesized a large-scale single-atomic graphene layer on Ni(111)/HOPG(0001). The Raman spectra also show a faint D band (~1350 cm^{-1}) associated with an almost negligible density of defects.[29] The Raman maps (Figure 3a—b), the high-resolution SEM image (Figure 3e), and the optical image (Figure 3f) of the graphene sheet on the SiO_2 substrate suggest the transferred graphene is highly homogeneous. The defective D peak may be associated with the defectlike points as observed in the SEM and optical images, which may be either inherent to the original graphene sheet and originated from grain boundary[34] or caused by the transfer[35] to the SiO_2/Si substrate since we found that transferring our graphene on the Ni/HOPG by the conventional etching method[14] is more difficult than transferring the graphene films synthesized on Ni/SiO_2/Si substrate. The difficulty in transferring our graphene might be due to a strong interaction of the graphene sheet with the HOPG substrate after etching away the Ni layer and to interaction of the poly(methyl methacrylate) (PMMA) coated on the graphene surface for transfer with the rough edges of the HOPG substrate in contrast to the sharp edges of a SiO_2/Si substrate.

The analysis of SEM images, Auger elemental maps, and AES spectra over the entire sample (2 cm × 2 cm) showed that macroscopic defects induced by holes, very bright protrusions, and grain boundaries are less than 1% in area (see Supporting Information, Figures S2—S3). Thus, our single-layer graphene sheet covers more than 99% of the entire Ni(111)/HOPG(0001) sample. All the Raman spectra collected from our graphene sample show single-layer characteristics based on the fwhm of the 2D band (~40 cm^{-1}), the peak intensity ratio I_G/I_{2D} (~0.31), and the single and sharp 2D peak, with the localized points where appear to be defective as pointed by an arrow (Figure 3b). It should be

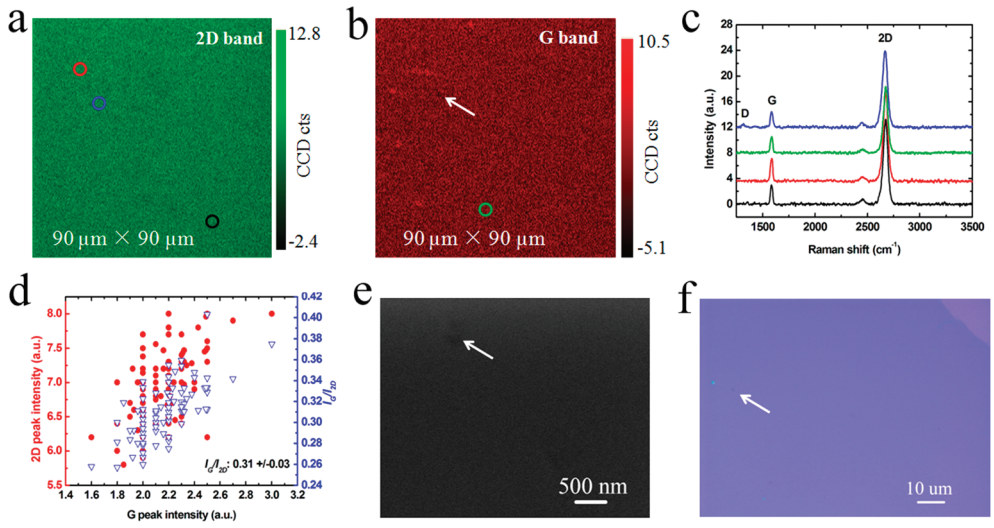

Figure 3. Characterization of graphene sheet transferred on SiO_2/Si, showing large-scale, uniform single-atomic graphene layer. (a) Raman 2D band (~2680 cm^{-1}). (b) Raman G band (~1580 cm^{-1}). (c) Raman spectra from marked spots with corresponding colored squares as in panels a and b; and a defective D band (~1350 cm^{-1}) appeared in one of the spectra. The Raman spectroscopy results were obtained from the graphene sheet transferred on a ~200 nm SiO_2 surface. (d) Scatter plots of Raman G peak intensity *versus* 2D peak intensity (bottom, left axis) and Raman G peak intensity *versus* the intensity G/2D ratio (bottom, right axis). The "I_G/I_{2D}: 0.31 ± 0.03" represents the G/2D intensity ratio with mean value of 0.31 and standard deviation of 0.03. (e) High-resolution SEM image of the graphene transferred on a ~300 nm SiO_2 surface. (f) High-resolution optical microscope image of the graphene transferred on a ~300 nm SiO_2 surface.

noted that the estimated 1% area covered by macroscopic defects can be further eliminated by optimizing the growth conditions together with improving the cleavage of the HOPG substrate. A poorly cleaved HOPG surface could affect the formation of the Ni(111) template, which in turn influences the continuity/quality of graphene synthesized on it (see Supporting Information, Figure S7). So far, no other methods have obtained such a nearly 100% coverage of single-layer graphene on a full Ni substrate,[36,37] on which commensurate epitaxial growth of structurally homogeneous graphene can be attained.

CONCLUSIONS

We provide a method for the synthesis of single-atomic layer epitaxial graphene covering almost 100% of a Ni(111)/HOPG(0001) surface at low temperatures (~650 °C) except for a few fractions associated with macroscopic defects. The sample size is easily scalable to large dimensions, limited only by the size of the substrate and the growth chamber. The graphene grown by the method presented here may be successfully transferred to other templates and achieves an almost 100% single-atomic layer graphene coverage of a desired substrate, either by intercalation methods[30] (to weaken the interaction between the metal substrate and the graphene layer) or by first separating the Ni substrate from the HOPG template and then etching away the Ni. Single-layer graphene has unique properties, such as very high mobility and an extraordinary quantum Hall effect, that bilayer and few-layer graphene films do not show.[1,38] We anticipate that the graphene grown with our method might have distinct transport characteristics due to the almost nonexistent lattice mismatch between HOPG(0001) and Ni(111), and between Ni and graphene; a characteristic that is drastically different from graphene sheets grown on silicon carbide,[10,11] copper,[15] ruthenium,[21,22] palladium,[24] iridium,[25] or platinum.[26] Despite this, the method is suitable for these metallic templates for producing graphene films with carbon atoms from a solid carbon source. Thus, graphene synthesized by this method may provide an interesting system for the exploration of relevant properties of nonmechanical exfoliated graphene and for practical large-scale applications. Our approach opens a new venue for guiding the graphene production process, as graphene films with high crystalline quality and uniform thickness are essential to realize unique electron transport for graphene-based technologies.

METHODS

Graphene Synthesis. A 100-nm-thick Ni film was deposited on a freshly cleaved HOPG(0001) substrate (SPI Supplies) by an E-gun evaporation system (RDEB-1206K, R-DEC Co. Ltd.) with a deposition rate of ~0.1 nm/s under a base pressure of ~7.5 × 10^{-8} Torr. The as-grown Ni on the HOPG(0001) (see Supporting Information, Figure S1) was annealed in a quartz tube for 6–30 h at 600–900 °C under a base pressure of ~5.0 × 10^{-8} Torr; subsequently, the temperature was decreased to 650 °C and maintained there for ~30 min; finally, the system was cooled to room temperature at a cooling rate of *ca.* 2–50 °C/min. We found that the treatment temperature and the time significantly

affect the formation of the Ni(111) surface, for example with respect to grain boundary and orientation, and in turn the quality of the graphene sheet. To synthesize uniform single-layer graphene on a Ni/HOPG substrate, it is essential to optimize the annealing temperature and annealing time. The main results in the article were obtained by treating the sample at 650 °C for 18 h and then allowing a cool down with a rate ~30 °C/min.

Graphene Wearing. To understand growth mechanism and to determine the thickness of our graphene sheet on Ni(111)/HOPG(0001), the sample was sputtered by rastering a focused 1.0 keV Ar^+ ion beam with a current of 0.1 μA over an area of 2 mm × 2 mm, and AES spectra were acquired from the center areas of the sputtered regions at several time intervals during the abrading process.

Graphene Transfer. For Raman spectroscopy characterization the graphene sheet on Ni substrate was transferred on a Si substrate with ~200 nm SiO_2 according to a previous report.[14] An ~500 nm poly(methyl methacrylate) (PMMA) was spin-coated on the surface of as-grown graphene layer on the Ni(111)/HOPG(0001) template. Subsequently, the Ni layer was etched away with a $FeCl_3$ (1 M) solution. The PMMA/graphene was then separated from the HOPG substrate with manual assistance and then placed on SiO_2/Si substrate. The PMMA/graphene sample transferred on the SiO_2/Si substrate was exposed to acetone to remove the top PMMA layer, washed by deionized water, and blow-dried with a N_2 gas gun. We found it more difficult to transfer the graphene from a Ni/HOPG template than from, for instance, a Ni/SiO_2/Si substrate using a similar protocol to the one described in ref 14. This peculiarity may be due to a stronger interaction of the graphene sheet with the HOPG substrate after etching away the Ni layer and to interactions with the rough edges of the HOPG substrate in contrast with the sharp edges of a SiO_2/Si template.

Scanning Auger Electron Spectroscopy. AES measurements simultaneously with scanning electron microscopy (SEM) were performed under ultrahigh vacuum (~1.0×10^{-10} Torr) at room temperature with a scanning Auger electron spectroscope (ULVAC-PHI model SAM650) with a cylindrical mirror analyzer.[32,33] The takeoff angle of the instrument was 42°. SEM images were acquired with a primary electron beam of 10 kV. The incident electron-beam current density for AES spectrum measurement was typically ~0.72 nA/μm^2. To subtract the background from the direct Auger spectrum, we used differential energy spectra. Differential $dN(E)/dE$ Auger spectra were obtained by numerical derivation of the direct $N(E)$−integrated Auger data displaying an absolute scale with counts/second units by a universal Savitzky−Golay differential filter using five points, which were used to calculate the peak-to-peak intensity of Auger electrons and to determine the thickness of the graphene layer on Ni. The differential spectrum is simply the differential of the direct spectrum with respect to energy. In the differential energy spectrum, it is customary to measure the peak-to-peak value of the signal. For the Auger transitions, for example, KLL, LMM, and MVV, measured in the present work, the K, L, and M represent the K, L, and M shell of an atom, respectively; the V represents the valence band of an atom. A KLL (or $KL_1L_{2,3}$) transition suggests an electron in the K shell is ionized by an incident beam, an electron in the L_1 shell fills the vacancy in the K shell, and the transition energy is imparted to another electron in the $L_{2,3}$ shell which is emitted. The negative peak positions of the C (carbon) KLL, the Ni (nickel) MVV, and the Ni LMM transitions in the differential spectrum are at 275, 64, and 849 eV, respectively.

Raman Spectroscopy. Raman spectra were recorded with a RAMAN-11 system (Nanophoton Corp., Japan), which illuminates a line-shaped area on the sample with a line-shaped laser beam. Raman scattering light from the line-shaped area on the sample was simultaneously detected by a parallel detection system.[32,39] The scattering signal was dispersed with a Czerny−Turner type spectrometer (f = 500 mm, the focal length of the spectrometer) and detected with an electrically cooled charge-coupled device (CCD) detector (400 pixels × 1340 pixels). The excitation source was a 532 nm laser with a power setting <1.0 mW to avoid laser-induced damage. The lateral resolution was ~350 nm focused by a ×100 optical lens (numerical aperture of 0.9), and the spectral resolution was ~1.6 cm^{-1}. From a Raman map, Raman spectrum at each pixel point can be collected and analyzed.

Atomic Force Microscopy (AFM). AFM images were acquired in amplitude-modulation mode (SPA400, SII Nanotechnologies, Japan) at room temperature in an ambient environment.[40] A supersharp tip with a radius of curvature of the tip of ~5 nm was used. Before measurement, the scan parameters such as the amplitude set point, integral and proportional gains, and scan rate were optimized.

Scanning Tunneling Microscopy (STM). STM images were recorded at tunneling conditions with bias of +0.3 V and tunneling current of 0.5 nA at 78 K using a low-temperature ultrahigh-vacuum STM system.[41,42] Prior to the observation, the sample (Ni/HOPG) was annealed at ~830 °C for ~21 h, and then the temperature was decreased to ~650 °C and maintained there for ~30 min in the STM chamber.

Acknowledgment. This work was partially supported by the budget for commission of MEXT, Japan, by the World Premier International Research Center Initiative (WPI Initiative) on Materials Nanoarchitectonics, MEXT, Japan, by the Fundamental Research Funds for the Central Universities, China (No. 2009QNA4046), and by the National Natural Science Foundation of China (Nos. 51011130028, 50990063, and 50973095). We thank O. Custance for advice on preparing the manuscript. The authors thank Nanophoton for support of Raman spectrum measurement, H. Gao for assistance of EBSD measurement, H. Iwai for maintenance of AES instrument, and J. H. Gao for kind help.

Supporting Information Available: AFM and SEM images of as-grown Ni film on HOPG, SEM images of graphene on Ni(111)/HOPG(0001), discussion of orientation of graphene on Ni grains by EBSD, AES characterization of graphene on Ni(111)/HOPG-(0001), estimation of carbon content in Ni film diffused from HOPG, helium ion image of graphene on a poorly prepared HOPG surface, and AES characterization of graphene film grown by the CVD method. This material is available free of charge *via* the Internet at http://pubs.acs.org.

REFERENCES AND NOTES

1. Geim, A. K.; Novoselov, K. S. The Rise of Graphene. *Nat. Mater.* **2007,** *6*, 183–191.
2. Xia, F.; Mueller, T.; Lin, Y. M.; Valdes-Garcia, A.; Avouris, Ph. Ultrafast Graphene Photodetector. *Nat. Nanotechnol.* **2009,** *4*, 839–843.
3. Lin, Y. M.; Dimitrakopoulos, C.; Farmer, D. B.; Chiu, H. Y.; Grill, A.; Avouris, Ph. 100-GHz Transistors from Wafer-Scale Epitaxial Graphene. *Science* **2010,** *327*, 662.
4. Yong, V.; Tour, J. M. Theoretical Efficiency of Nanostructured Graphene-Based Photovoltaics. *Small* **2010,** *6*, 313–318.
5. Xu, M. S.; Fujita, D.; Hanagata, N. Perspectives and Challenges of Emerging Single-Molecule DNA Sequencing Technologies. *Small* **2009,** *5*, 2638–2649.
6. Partoens, B.; Peeters, F. M. From Graphene to Graphite: Electronic Structure around the *K* Point. *Phys. Rev. B* **2006,** *74*, 075404.
7. Lahiri, J.; Lin, Y.; Bozkurt, P.; Oleynik, I. I.; Batzill, M. An Extended Defect in Graphene as a Metallic Wire. *Nat. Nanotechnol.* **2010,** *5*, 326–329.
8. Hernandez, Y.; Nicolosi, V.; Lotya, M.; Blighe, F. M.; Sun, Z.; De, S.; McGovern, I. T.; Holland, B.; Byrne, M.; Gun'Ko, Y. K.; *et al.* High-Yield Production of Graphene by Liquid-Phase Exfoliation of Graphite. *Nat. Nanotechnol.* **2008,** *3*, 563–568.
9. Li, X. L.; Zhang, G. Y.; Bai, X. D.; Sun, X. M.; Wang, X. R.; Wang, E. G.; Dai, H. J. Highly Conducting Graphene Sheets and Langmuir−Blodgett Films. *Nat. Nanotechnol.* **2008,** *3*, 538–542.
10. Berger, C.; Song, Z. M.; Li, T. B.; Li, X. B.; Ogbazghi, A. Y.; Feng, R.; Dai, Z. T.; Marchenkov, A. N.; Conrad, E. H.; First, P. N.; *et al.* Ultrathin Epitaxial Graphite: 2D Electron Gas

Properties and a Route toward Graphene-Based Nanoelectronics. *J. Phys. Chem. B* **2004,** *108*, 19912–19916.
11. Emtsev, K. V.; Bostwick, A.; Horn, K.; Jobst, J.; Kellogg, G. L.; Ley, L.; McChesney, J. L.; Ohta, T.; Reshanov, S. A.; Röhrl, J.; *et al*. Towards Wafer-Size Graphene Layers by Atmospheric Pressure Graphitization of Silicon Carbide. *Nat. Mater.* **2009,** *8*, 203–207.
12. Yu, Q. K.; Lian, J.; Siriponglert, S.; Li, H.; Chen, Y. P.; Pei, S. S. Graphene Segregated on Ni Surfaces and Transferred to Insulators. *Appl. Phys. Lett.* **2008,** *93*, 113103.
13. Reina, A.; Jia, X. T.; Ho, J.; Nezich, D.; Son, H.; Bulovic, V.; Dresselhaus, M. S.; Kong, J. Large Area, Few-Layer Graphene Films on Arbitrary Substrates by Chemical Vapor Deposition. *Nano Lett.* **2009,** *9*, 30–35.
14. Kim, K. S.; Zhao, Y.; Jang, H.; Lee, S. Y.; Kim, J. M.; Kim, K. S.; Ahn, J. H.; Kim, P.; Choi, J. Y.; Hong, B. H. Large-Scale Pattern Growth of Graphene Films for Stretchable Transparent Electrodes. *Nature* **2009,** *457*, 706–710.
15. Li, X. S.; Cai, W. W.; An, J. H.; Kim, S.; Nah, J.; Yang, D. X.; Piner, R.; Velamakanni, A.; Jung, I.; Tutuc, E.; *et al*. Large-Area Synthesis of High-Quality and Uniform Graphene Films on Copper Foils. *Science* **2009,** *324*, 1312–1314.
16. Shelton, J. C.; Patil, H. R.; Blakely, J. M. Equilibrium Segregation of Carbon to a Nickel (111) Surface: A Surface Phase Transition. *Surf. Sci.* **1974,** *43*, 493–520.
17. Fujita, D.; Yoshihara, K. Surface Precipitation Process of Epitaxially Grown Graphite (0001) Layers on Carbon-Doped Nickel(111) Surface. *J. Vac. Sci. Technol., A* **1994,** *12*, 2134–2139.
18. Gao, J. H.; Fujita, D.; Xu, M. S.; Onishi, K.; Miyamoto, S. Unique Synthesis of Few-Layer Graphene Films on Carbon-Doped $Pt_{83}Rh_{17}$ Surface. *ACS Nano* **2010,** *4*, 1026–1032.
19. Li, S. X.; Zhu, Y. W.; Cai, W. W.; Borysiak, M.; Han, B. Y.; Chen, D.; Piner, R. D.; Colombo, L.; Ruoff, R. S. Transfer of Large-Area Graphene Films for High-Performance Transparent Conductive Electrodes. *Nano Lett.* **2009,** *9*, 4359–4363.
20. Bae, S.; Kim, H.; Lee, Y.; Xu, X. F.; Park, J. S.; Zheng, Y.; Balakrishnan, J.; Lei, T.; Kim, H. R.; Song, Y. I.; *et al*. Roll-to-Roll Production of 30-in. Graphene Films for Transparent Electrodes. *Nat. Nanotechnol.* **2010,** *5*, 574–578.
21. Sutter, P. W.; Flege, J. I.; Sutter, E. A. Epitaxial Graphene on Ruthenium. *Nat. Mater.* **2008,** *7*, 406–411.
22. Pan, Y.; Zhang, H. G.; Shi, D. X.; Sun, J. T.; Du, S. X.; Liu, F.; Gao, H. J. Highly Ordered, Millimeter-Scale, Continuous, Single-Crystalline Graphene Monolayer Formed on Ru (0001). *Adv. Mater.* **2009,** *21*, 2777–2780.
23. Reina, A.; Thiele, S.; Jia, X. T.; Bhaviripudi, S.; Dresselhaus, M. S.; Schaefer, J. A.; Kong, J. Growth of Large-Area Single and Bi-layer Graphene by Controlled Carbon Precipitation on Polycrystalline Ni Surfaces. *Nano Res.* **2009,** *2*, 509–516.
24. Kwon, S. Y.; Ciobanu, C. V.; Petrova, V.; Shenoy, V. B.; Bareno, J.; Gambin, V.; Petrov, I.; Kodambaka, S. Growth of Semiconducting Graphene on Palladium. *Nano Lett.* **2009,** *9*, 3985–3990.
25. Coraux, J.; N'Diaye, A. T.; Busse, C.; Michely, T. Structural Coherency of Graphene on Ir(111). *Nano Lett.* **2008,** *8*, 565–570.
26. Sutter, P. W.; Sadowski, J. T.; Sutter, E. A. Graphene on Pt(111): Growth and Substrate Interaction. *Phys. Rev. B* **2009,** *80*, 245411.
27. Hembacher, S.; Giessibl, F. J.; Mannhart, J.; Quate, C. F. Revealing the Hidden Atom in Graphite by Low-Temperature Atomic Force Microscopy. *Proc. Natl. Acad. Sci. U.S.A.* **2003,** *100*, 12539–12542.
28. Murata, Y.; Petrova, V.; Kappes, B. B.; Ebnonnasir, A.; Patrov, I.; Xie, Y. H.; Ciobanu, C. V.; Kodambaka, S. Moire Superstructures of Graphene on Faceted Nickel Islands. *ACS Nano* **2010,** *4*, 6509–6514.
29. Ferrari, A. C.; Meyer, J. C.; Scardaci, V.; Casiraghi, C.; Lazzeri, M.; Mauri, F.; Piscanec, S.; Jiang, D.; Novoselov, K. S.; Roth, S.; *et al*. Raman Spectrum of Graphene and Graphene Layers. *Phys. Rev. Lett.* **2006,** *97*, 187401.
30. Nagashima, A.; Tejima, N.; Oshima, C. Electronic States of the Pristine and Alkali-Metal-Intercalated Monolayer Graphite/Ni(111) Systems. *Phys. Rev. B* **1994,** *50*, 17487.
31. Ohtani, H.; Hasebe, M.; Nishizawa, T. Calculation of Fe−C, Co−C and Ni−C Phase Diagrams. *Trans. ISIJ* **1984,** *24*, 857–864.
32. Xu, M. S.; Fujita, D.; Gao, J. H.; Hanagata, N. Auger Electron Spectroscopy: A Rational Method for Determination of Thickness of Graphene Films. *ACS Nano* **2010,** *4*, 2937–2945.
33. Briggs, D., Seah, M. P., Eds. *Practical Surface Analysis: Auger and X-ray Photoelectron Spectroscopy*; John Wiley & Sons: New York, 1990.
34. Li, X. S.; Magnuson, C. W.; Venugopal, A.; An, J. H.; Suk, J. W.; Han, B. Y.; Borysiak, M.; Cai, W. W.; Velamakanni, A.; Zhu, Y. W.; *et al*. Graphene Films with Large Domain Size by a Two-Step Chemical Vapor Deposition Process. *Nano Lett.* **2010,** *10*, 4328–4334.
35. Levendori, M. P.; Ruiz-Vargas, C. S.; Garg, S.; Park, J. Transfer-free Batch Fabrication of Single Layer Graphene Transistors. *Nano Lett.* **2009,** *9*, 4479–4483.
36. Zhu, Y. W.; Murali, S.; Cai, W. W.; Li, X. S.; Suk, J. W.; Potts, J. R.; Ruoff, R. S. Graphene and Graphene Oxide: Synthesis, Properties, and Applications. *Adv. Mater.* **2010,** *22*, 3906–3924.
37. Sun, Z. Z.; Yan, Z.; Yao, J.; Beitler, E.; Zhu, Y.; Tour, J. M. Growth of Graphene from Solid Carbon Sources. *Nature* **2010,** *468*, 549–552.
38. Craciun, M. F.; Russo, S.; Yamamoto, M.; Oostinga, J. B.; Morpurgo, A. F.; Tarucha, S. Trilayer Graphene is a Semimetal with a Gate-Tunable Band Overlap. *Nat. Nanotechnol.* **2009,** *4*, 383–388.
39. Xu, M. S.; Fujita, D.; Hanagata, N. Monitoring Electron-Beam Irradiation Effects on Graphenes by Temporal Auger Electron Spectroscopy. *Nanotechnology* **2010,** *21*, 265705.
40. Xu, M. S.; Fujita, D.; Onishi, K. Reconstruction of Atomic Force Microscopy Image by Using Nanofabricated Tip Characterizer toward the Actual Sample Surface Topography. *Rev. Sci. Intrum.* **2009,** *80*, 043703.
41. Sagisaka, K.; Fujita, D.; Kido, G. Phase Manipulation between $c(4 \times 2)$ and $p(2 \times 2)$ on the Si(100) Surface at 4.2 K. *Phys. Rev. Lett.* **2003,** *91*, 146103.
42. Xu, M. S.; Endres, R. G.; Arakawa, Y. The Electronic Properties of DNA Bases. *Small* **2007,** *3*, 1539–1543.